Rare Met. (2017) 36(4):289–294
DOI 10.1007/s12598-017-0888-7

RARE METALS
www.editorialmanager.com/rmet

Numerical analysis of solid–liquid interface shape during large-size single crystalline silicon with Czochralski method

Ran Teng, Qing Chang*, Yang Li, Bin Cui, Qing-Hua Xiao, Guo-Hu Zhang

Received: 12 November 2016 / Revised: 27 December 2016 / Accepted: 4 February 2017 / Published online: 15 March 2017

Abstract Numerical analysis is an effective tool to research the industrial Czochralski (CZ) crystal growth aiming to improve crystal quality and reduce manufacturing costs. In this study, a set of global simulations were carried out to investigate the effect of crystal-crucible rotation and pulling rate on melt convection and solid–liquid (SL) interface shape. Through analyses of the simulation data, it is found that the interface deformation and inherent stress increase during the crystal growth process. The interface deflection increases from 7.4 to 51.3 mm with an increase in crystal size from 150 to 400 mm. In addition, the SL interface shape and flow pattern are sensitive to pulling rate and rotation rate. Reducing pulling rate can flat SL interface shape and add energy-consuming. Interface with low deflection can be achieved by adopting certain combination of crystal and crucible rotation rates. The effect of crystal rotation on SL interface shape is less significant at higher crucible rotation rates.

Keywords Czochralski method; Numerical analysis; Pull rate; Crucible rotation; Crystal rotation; Solid/liquid interface shape

R. Teng, Q. Chang*, Y. Li, B. Cui, Q.-H. Xiao, G.-H. Zhang
National Engineering Research Center for Semiconductor Materials, Beijing 100088, China
e-mail: changqing@gritek.com

R. Teng
General Research Institute for Nonferrous Metals, Semiconductor Materials Co., Ltd, Beijing 100088, China

1 Introduction

The Czochralski (CZ) growth process is the main method for single crystalline silicon preparation in microelectronic and photovoltaic industry. To meet the requirements of a high degree of integration and semiconductor devices quality, it is essential to understand the transport phenomena and the fluid flow motions in melt. Owing to the high-temperature environment and high cost, experimental investigation and in situ observation are quite difficult. Therefore, numerical analysis is considered to be a very beneficial and effective tool in analysis of CZ silicon crystal growth, especially on heat transfer and mass transport.

The crystal diameter from 150 to 400 mm requires 32-inch-quartz crucible or even more. Therefore, the crystal preparation needs a large sum of polycrystalline silicon in crucible, which means larger fluid turbulent and temperature fluctuation. The solid–liquid (SL) interface shape is a key question in large diameter crystal growth process, which can influence the crystallization rate, crystal inherent stress or even point defect behavior. Though massive efforts have been done by industry to control SL interface shape, the theory and experience from small size crystal can be adopted partially. With quartz crucible size and crystal diameter increasing, temperature distribution and melt flow indicate the character of size effect. Therefore, it is essential to investigate the effect of key processing parameters, such as crystal-crucible rotation and pulling rate, on SL interface shape.

So far, domestic and overseas scholars have done a lot of researches on melt flow and SL interface shape with different process parameters and furnace configuration. Chen et al. [1, 2] calculated oxygen concentration

distribution in silicon melt for different crystal lengths with magnetic field using simulator CGSim. The hot zone structure was optimized [3–12], such as heat-shield, flow guide and sidewall insulation. The results showed that the optimized hot zone can increase the growth rate and crystal quality. The effect of gas flow on global heat transport and melt convection in CZ-Si growth was also studied [13–16], and the cause of W-shape SL interface formation was analyzed [17–19]. Wetzel et al. [20, 21] predicted the growth interface shape in industrial 300 mm CZ-Si crystal growth. Lukanin et al. [22] and Dadzis et al. [23] presented an updated version of the combined 2D/3D model of heat transfer and turbulent melt convection for industry CZ crystal growth. Then, the complex flow during CZ-Si crystal growth process was predicted [24–29]. Yi et al. studied the flow patterns within a large-scale CZ system, using 3-D time-dependent numerical model [30, 31].

The aim in this paper is to investigate the effect of pulling rate and crystal-crucible rotation rate on SL interface shape and find out a proper process route and solution. Different body lengths were considered to evaluate the variation of the optimum control parameters during CZ-Si crystal growth process.

2 Model constructions

The modeling of mass transport and heat transfer in the furnace of KAYEX-150 was analyzed by finite element method (FEM) adopting 2-D axial-symmetric model. The melt flow and heat transfer were governed by the following equations:

$$\rho_0 \cdot (v \cdot \nabla)v = -\nabla p + \nabla \cdot \left((\mu + \mu_{\mathrm{T}})(\nabla v + \nabla^{\mathrm{T}} v)\right) - \rho_0 \beta_{\mathrm{T}}(T - T_0)g + J \times B \quad (1)$$

$$\nabla \cdot v = 0 \quad (2)$$

$$\rho_l c\left(\frac{\partial T}{\partial t} + (v \cdot \nabla)T\right) = \nabla \cdot ((k + k_{\mathrm{T}})\nabla T) + W \quad (3)$$

$$-k_l \nabla T_l \cdot n = -k_s \nabla T_s \cdot n - \rho_s v_{\mathrm{g}} \Delta H \quad (4)$$

$$T_{\mathrm{triple}} = 1685\ \mathrm{K} \quad (5)$$

Here, v is velocity, B is magnetic field intensity, μ is coefficient of the melt viscosity, μ_{T} is coefficient of the melt viscosity under magnetic field, β_{T} is the coefficient of thermal expansion, J is current density, ρ_0 is melt density, p is pressure, T_0 is reference temperature, g is acceleration of gravity, k is thermal conductivity, k_{T} is thermal conductivity under magnetic field, W is heater power, ρ_{l} is density of melt, ρ_s is density of crystal, c is specific heat, T is temperature, T_l is melt temperature, T_s is crystal temperature, T_{triple} is triple point temperature, ΔH is crystallization enthalpy, k_l is heat conductivity of melt, k_s is heat conductivity of crystal, v_{g} is crystal growth rate, n is the unit outgoing normal from the melt, ∇ is differential operator.

Boundary conditions for the flow velocity at the solid walls were as follows: the velocity component perpendicular to the wall was set to zero, while the tangential components were equal to the solid wall velocity. The Reynolds-averaged Navier–Stokes (RANS) equations were applied to solve turbulent flow. At the outer walls of the facility, a constant temperature value was adopted as boundary conditions. The grids in the present finite element analysis were constructed as follows: auto splitting for radiative modeling uses 10 mm separations globally; crystal and melt have structured grids near the crystallization interface in 6 mm separations; the crystal and melt that are not adjacent to the interface use triangular grids also in 6 mm separations with stretching coefficient of 1.1 in Delaunay method; parts other than the crystal and melt use triangular grids in 10 mm separations with stretching coefficient of 1.25.

The drawing of Kayex-150 single crystal furnace and the temperature distribution in the growth facility obtained with the 2-D global heat computations are presented in Fig. 1. The material properties utilized in the present computations are summarized in Table 1.

3 Results and discussion

The computational results in this section present the growth of 400-mm-diameter crystals with 32-inch-crucible in an industrial CZ silicon puller. The multi-block combined grid consists of about 19,200 cells and contains mismatched

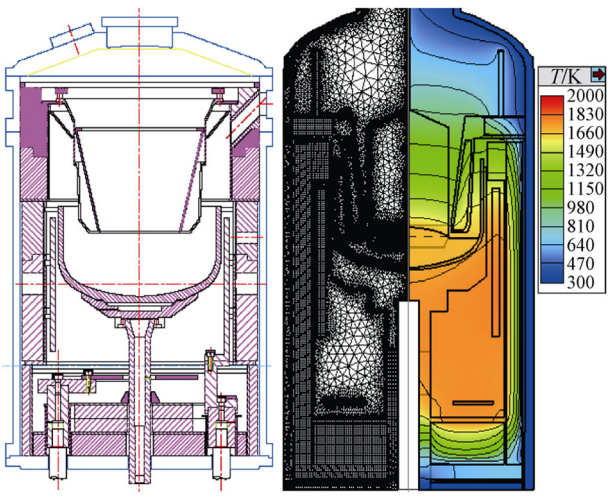

Fig. 1 Drawing of Kayex-150 single crystal furnace (left) and computational grid and temperature distributions (right) in growth system obtained with 2-D global heat computations (right)

Table 1 Material properties used in simulation

Materials	Emissivity	λ_{eff}/(W·m^{-1}·K^{-1})	Density/(kg·m^{-3})	c_p/(J·kg^{-1}·K^{-1})	Melting temperature/K
Si crystal	$0.9–2.6 \times 10^{-4}T$	$98.9–0.09T + 2.89 \times 10^{-5}T^2$	$2330–2.19 \times 10^{-8}T$	$687 + 0.236T$	1685
Si melt	0.171	66.5	$2332 + 0.48T–1.98 \times 10^{-4}T^2$	915	–
Graphite	0.800	$146.9–0.177T + 1.27 \times 10^{-4}T^2$	–	–	–
Insulator	0.900	–	–	–	–
Quartz	0.850	4.0	–	–	–
Steel	0.450	15.0	–	–	–
Argon	–	$0.01 + 2.5 \times 10^{-5}T$	–	–	–

λ_{eff}, Effective thermal conductivity; c_p, Specific heat

boundaries at SL interface. The control parameters for the crystal growth are as follows: the polycrystalline silicon charge amount is 220 kg, the crystal rotation is 8 r·min^{-1}, the crucible rotation is 10 r·min^{-1}, the argon flow rate is 0.002 m^3·min^{-1}, and the pressure of the furnace is 2000 Pa.

3.1 Effect of crystal size and body length on SL interface shape

During crystal growth, the melt flow in the crucible plays a crucial role in terms of crystal quality and dopant variation. Figure 2 illustrates SL interface shape at body lengths of 10, 100, 200 and 310 mm. SL interface shape switches from gull-wing shape to convex and the maximum deflection increases significantly with the crystal growth process going. Generally speaking, the flow pattern is driven by the buoyancy generated by the temperature difference within the melt, the crystal and crucible rotations, the shear stress generated by the argon flow, the capillary stress and the Marangoni stress at the melt free surface. Based on the calculations and the reported studies [13, 32], the effects of Marangoni stress, capillary stress and shear stress are ignored compared to other effects. Therefore, here it was only discussed the effects of key driving forces in the melt flow (the buoyancy, crucible-crystal rotations and crystal pull rate).

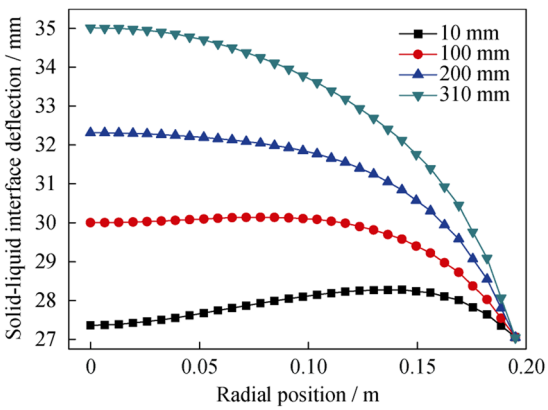

Fig. 2 Solid–liquid interface deflection for different body lengths

Figure 3 shows meridional cut through the melt with distribution of the stream traces for different body lengths. When the body lengths reach 10 and 100 mm, there is only one counter-clockwise vortex in the melt. It rises from the bottom along the crucible side and transports to the center at the surface and then flows to bottom. As the body length reaches 200 mm, the flow pattern in the melt starts to change. A small new vortex generates under SL interface. The two vortices have the opposite direction of movement. As the body length reaches 310 mm, the strength and size of the new vortex increase, leading to interface deflection. Overall, with the crystal growth processing, the new vortex becomes bigger and stronger. So the heat input is increased under the interface, the shape of the interface will move up.

High thermal stress (von Misses stress) in the crystal is one of the most possible reasons to generate dislocation. Figure 4 shows thermal stress distributions at the body

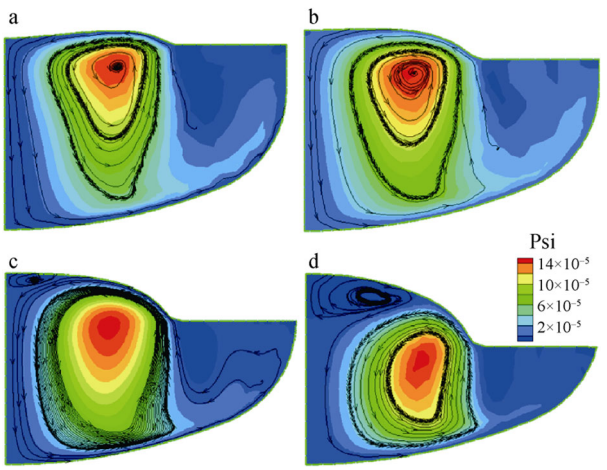

Fig. 3 Stream functions and streamlines for different body lengths: **a** 10 mm, **b** 100 mm, **c** 200 mm, and **d** 310 mm (Psi: pounds per square inch)

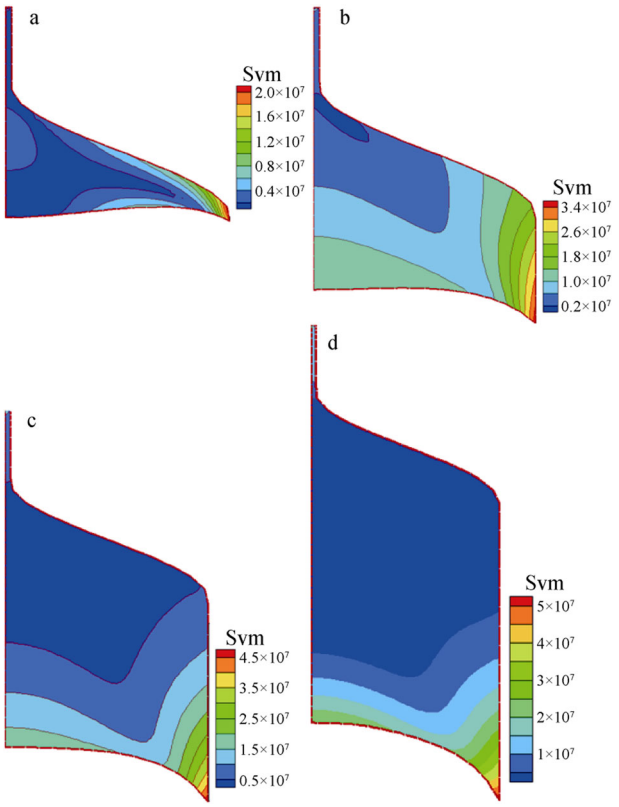

Fig. 4 Von Mises stress distribution for different body lengths: **a** 10 mm, **b** 100 mm, **c** 200 mm, and **d** 310 mm (Svm: stress of von mises)

lengths of 10, 100, 200 and 310 mm. The calculation of the thermal stress is based upon the computation data of temperature distribution. The results show that the thermal stress of the crystal is relying heavily on body length. With the crystal process going, the maximum von Misses stress rapidly increases, which is located at the SL interface and the crystal side surface. Owing to the large interface deformation, the high stress value appears at the SL interface when the crystal growth reaches 310 mm.

3.2 Effect of crystal-crucible rotation rates on SL interface shape

The region of maximum SL interface deformation will become the stress concentration point. It means that the intensity of the thermo-elastic stress concentration is in proportion to the degree of interface deflection. Therefore, it is essential to investigate how the crystal and crucible rotation rates affect maximum interface deflection. Figure 5 illustrates the effect of crystal size on SL interface shape. The SL interface deflection increases from 7.4 to 51.3 mm with an increase in crystal size from 150 to 400 mm. As the crystal size gets larger, the maximum SL interface shape deformation rapidly increases.

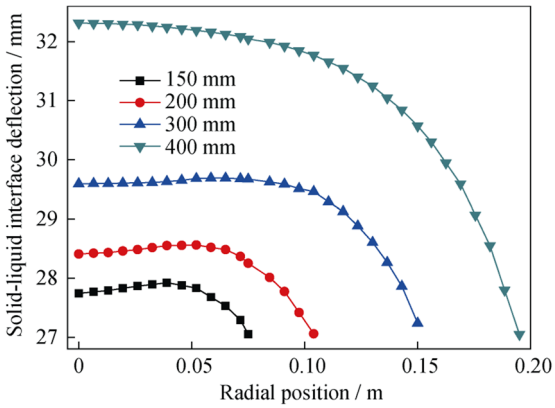

Fig. 5 Solid–liquid interface deflection with different crystal diameters

Figure 6 illustrates the combined effects of crystal and crucible rotation rates on the maximum interface deflection. It can be seen that the SL interface shape deflection is smaller for higher crucible rotation rates. The minimum point of interface deflection is closely related to the combinations of crystal and crucible rotation rates. It means that improving the quality in terms of the behavior of the melt flow or the shape of the SL interface can be achieved through the selected combinations of crystal and crucible rotation rates. For current furnace geometry and control parameters, the minimum interface deflection appears when the crystal rotation rates are between 4 and 8 $r \cdot min^{-1}$ and crucible rotation rate is 15 $r \cdot min^{-1}$ for 100 mm body length. The maximum deformation mostly increases with body length increasing. However, the minimum value still exists, as shown in Fig. 6. The curve for crucible rotation rate of 5 $r \cdot min^{-1}$ shows parabolic trend with a distinct minimum point. The curves for crucible rotation rates of 10 and 15 $r \cdot min^{-1}$ are nearly flat. After reaching the minimum point, the effect of crystal rotation on the interface is less significant at higher crucible rotation rates. This is more distinct for 310 mm body length, as shown in Fig. 6 (and also for 400 mm body length, although not shown here).

3.3 Effect of pulling rate on SL interface shape

In a CZ furnace, the crystallization takes place at the SL interface. This interface is also called the crystallization front. The SL interface shape directly influences the crystalline perfection and the impurity distribution. The convex shape (viewed from the crystal side) is prone to generate dislocations. As the pulling rate increases, the SL interface gradually changes to the concave shape, as shown in Fig. 7.

The growth rate of crystal, everyplace at the interface, is equal to the axial pulling rate at body growth. During the process of crystallization, the latent heat will release at the crystallization front. The faster the crystal we pull from

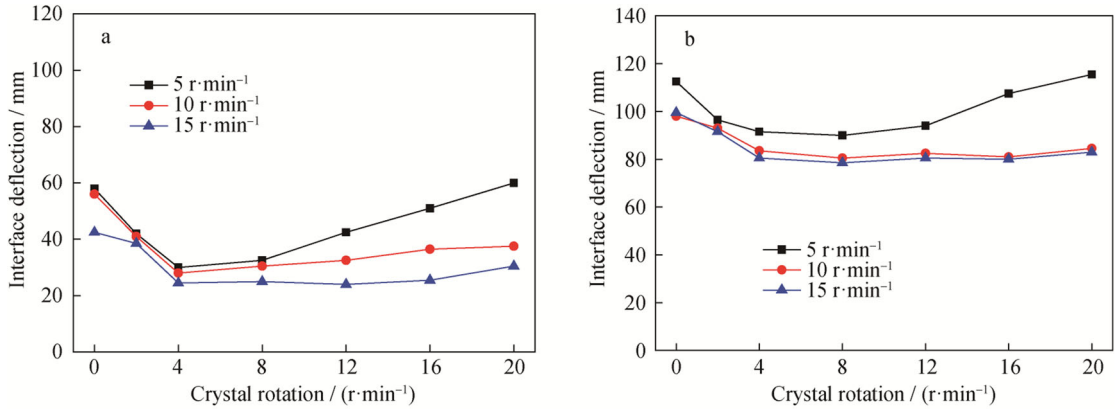

Fig. 6 Maximum solid–liquid interface deflection for lengths of **a** 100 mm and **b** 310 mm with various combinations of crystal and crucible rotation rates

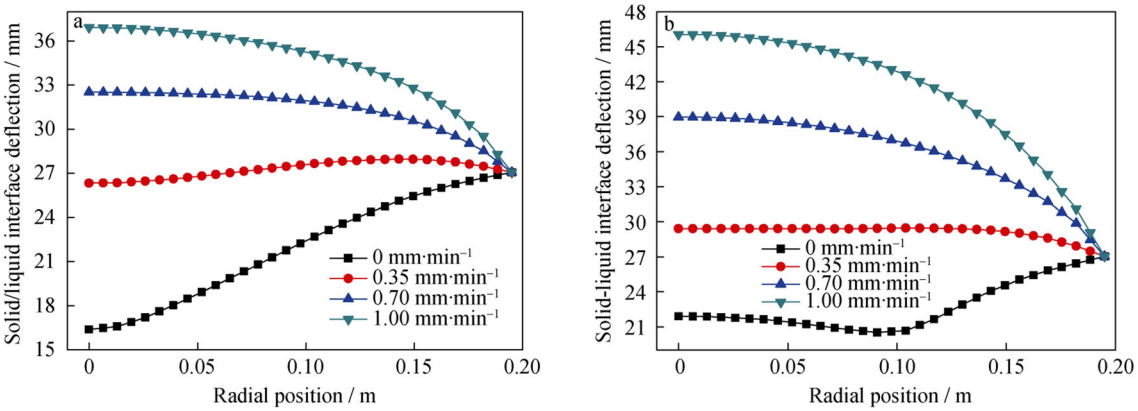

Fig. 7 Solid–liquid interface deflection for lengths of **a** 100 mm and **b** 310 mm with various pulling rates

melt, the more the latent heat will release. The heat power reduces by 4.2 kW with an increase in the pull rate from 0.35 to 1.00 mm·min^{-1}. The change in the heater power leads to the temperature field fluctuation in CZ furnace.

The temperature in the furnace decreases because of the reducing heater power. With an increase in pulling rate, more latent heat is released at the crystallization front and must be conducted away into crystal. This is accomplished partly through decreasing heat power and partly by increasing interface deflection. If the heat input is increased, the shape of the SL interface will move up. If the heat input is decreased, the SL interface will move down closer to the melt level. The interface height increases by 8 mm with an increase in the pull rate from 0.35 to 1.00 mm·min^{-1}.

4 Conclusion

In this study, a set of numerical simulations were carried out to investigate the change rules of melt flow and SL interface geometry for different control parameters. With crystal diameter increasing, the SL interface deflection increases accordingly. The SL interface deformation and the maximum thermal stress continue to increase with the crystallization going. The stress concentration mainly locates at the crystallization front and the crystal side surface. The SL interface shape is sensitive to both crucible and crystal rotation rates. The optimal combination of crystal and crucible rotations slightly changes during the crystal growth process. The maximum SL interface shape deflection increases with the crystal rotation rate accelerating and decreases with the crucible rotation rate speeding. The lowest SL interface deflection can be realized through optimizing the combination of crucible and crystal rotation. In addition, reducing pulling rate can flat SL interface shape and subsequently add energy-consuming.

Acknowledgements This study was financially supported by the Major National Science and Technology Projects (No. 2009ZX02011).

References

[1] Chen JC, Chiang PY, Chang CH, Teng YY, Huang CC, Chen CH, Liu CC. Three-dimensional numerical simulation of flow, thermal and oxygen distributions for a Czochralski silicon growth with in a transverse magnetic field. J Cryst Growth. 2014;401(1):813.

[2] Chen JC, Chiang PY, Nguyen TH, Hu C, Chen CH, Liu CC. Numerical simulation of the oxygen concentration distribution in silicon melt for different crystal lengths during Czochralski growth with a transverse magnetic field. J Cryst Growth. 2016; 452(15):6.

[3] Zhao WH, Liu LJ. Control of heat transfer in continuous-feeding Czochralski-silicon crystal growth with a water-cooled jacket. J Cryst Growth. 2017;458(15):31.

[4] Prostomolotov AI, Verezub NA, Mezhennii MV, Reznik VY. Thermal optimization of CZ bulk growth and wafer annealing for crystalline dislocation-free silicon. J Cryst Growth. 2011; 318(1):187.

[5] Su WJ, Zuo R, Mazaev K, Kalaev V. Optimization of crystal growth by changes of flow guide, radiation shield and sidewall insulation in Cz Si furnace. J Cryst Growth. 2010;312(4):495.

[6] Smirnova OV, Durnev NV, Shandrakova KE, Mizitov EL, Soklakov VD. Optimization of furnace design and growth parameters for Si Cz growth, using numerical simulation. J Cryst Growth. 2008;310(7–9):2185.

[7] Huang LY, Lee PC, Hsieh CK, Hsu WC, Lan CW. On the hot-zone design of Czochralski silicon growth for photovoltaic applications. J Cryst Growth. 2004;261(2):433.

[8] Daggolu P, Ryu JW, Galyukov A, Kondratyev A. Analysis of the effect of symmetric/asymmetric CUSP magnetic fields on melt/crystal interface during Czochralski silicon growth. J Cryst Growth. 2016;452(15):22.

[9] Vizman D, Dadzis A, Friedrich J. Numerical parameter studies of 3D melt flow and interface shape for directional solidification of silicon in a traveling magnetic field. J Cryst Growth. 2013; 381(15):169.

[10] Zhao W, Liu L. Control of heat transfer in continuous-feeding Czochralski-silicon crystal growth with a water-cooled jacket. J Cryst Growth. 2016;458(15):31.

[11] Sim BC, Jung YH, Lee JE, Lee HW. Effect of the crystal–melt interface on the grown-in defects in silicon CZ growth. J Cryst Growth. 2007;299(1):152.

[12] Liu X, Nakano S, Kakimoto K. Effect of the packing structure of silicon chunks on the melting process and carbon reduction in Czochralski silicon crystal growth. J Cryst Growth. 2016. doi: 10.1016/j.jcrysgro.2016.09.062.

[13] Kalaev VV, Evstratov IY, Makarovb YN. Gas flow effect on global heat transport and melt convection in Czochralski silicon growth. J Cryst Growth. 2003;249(1–2):87.

[14] Fang HS, Jin ZL, Huang XM. Study and optimization of gas flow and temperature distribution in a Czochralski configuration. J Cryst Growth. 2012;361(24):114.

[15] Li ZY, Liu LJ, Liu X, Zhang YF, Xiong JF. Effects of argon flow on melt convection and interface shape in a directional solidification process for an industrial-size solar silicon ingot. J Cryst Growth. 2012;360(1):87.

[16] Sabanskis A, Virbulis J. Simulation of the influence of gas flow on melt convection and phase boundaries in FZ silicon single crystal growth. J Cryst Growth. 2015;417(1):51.

[17] Noghabi OA, Jomaa M, Mhamdi M. Analysis of W-shape melt/crystal interface formation in Czochralski silicon crystal growth. J Cryst Growth. 2013;362(1):77.

[18] Noghabi OA, Hamdi MM, Jomaa M. Effect of crystal and crucible rotations on the interface shape of Czochralski grown silicon single crystals. J Cryst Growth. 2011;318(1):173.

[19] Fujiwara K, Gotoh R, Yang XB, Koizumi H, Nozawa J, Uda S. Morphological transformation of a crystal–melt interface during unidirectional growth of silicon. Acta Mater. 2011;59(11):4700.

[20] Wetzel T, Muiznieks A, Muhlbauer A, Gelfgat Y, Gorbunov L, Virbulis J, Tomzig E, Ammon WV. Numerical model of turbulent CZ melt flow in the presence of AC and CUSP magnetic fields and its verification in a laboratory facility. J Cryst Growth. 2001;230(1–2):81.

[21] Wetzel T, Virbulis J, Muiznieksc A, Ammon WV, Tomzig E, Raming G, Webera M. Prediction of the growth interface shape in industrial 300 mm CZ Si crystal growth. J Cryst Growth. 2004;266(1–3):34.

[22] Lukanin DP, Kalaev VV, Makarov YN, Wetzel T, Virbulis J, Ammon WV. Advances in the simulation of heat transfer and prediction of the melt–crystal interface shape in silicon CZ growth. J Cryst Growth. 2004;266(1):20.

[23] Dadzis K, Vizman D, Friedrich J. Unsteady coupled 3D calculations of melt flow, interface shape, and species transport for directional solidification of silicon in a traveling magnetic field. J Cryst Growth. 2013;367(15):77.

[24] Shiraishi Y, Maeda S, Nakamura K. Prediction of solid liquid interface shape during CZ Si crystal growth using experimental and global simulation. J Cryst Growth. 2004;266(1–3):28.

[25] Abe T, Takahashi T, Shirai K, Zhang XW. Investigations of interstitial generations near growth interface depending on crystal pulling rates during CZ silicon growth by detaching from the melt. J Cryst Growth. 2016;434(15):128.

[26] Vegad M, Bhatt NM. Effect of location of zero gauss plane on oxygen concentration at crystal melt interface during growth of magnetic silicon single crystal using Czochralski technique. Proced Technol. 2016;23:480.

[27] Li YR, Akiyama Y, Imaishi N, Tsukada T. Global analysis of a small Czochralski furnace with rotating crystal and crucible. J Cryst Growth. 2003;255(1–2):81.

[28] Li YR, Wu CM, Wu SY, Peng L. Three-dimensional flow driven by iso and counter-rotation of a shallow pool and a disk on the free surface. Phys Fluids. 2009;21(8):084102.

[29] Li YR, Yuan XF, Wu CM, Hu YP. Natural convection of water near its density maximum between horizontal cylinder. Int J Heat Mass Transf. 2011;54(11):2250.

[30] Son SS, Yi KW. Experimental study on the effect of crystal and crucible rotations on the thermal and velocity field in a low Pra'ndtl number melt in a large crucible. J Cryst Growth. 2010; 275(1–2):249.

[31] Nam PO, Yi KW. 3-D time-dependent numerical model of flow patterns within a large-scale Czochralski system. J Cryst Growth. 2008;310(7–9):2126.

[32] Muiznieks A, Krauze A, Nacke B. Convective phenomena in large melts including magnetic fields. J Cryst Growth. 2007; 303(1):211.